Inhibition of the ROS-mediated cytotoxicity and genotoxicity of nano-TiO2 toward human keratinocyte cells by iron doping

Mara Ghiazza • Elisa Alloa • Simonetta Oliaro-Bosso • Franca Viola •Stefano Livraghi • Diana Rembges • Robin Capomaccio •Franc¸ois Rossi • Jessica Ponti • Ivana Fenoglio

Inhibition of the ROS-mediated cytotoxicity and genotoxicity of nano-TiO_2 toward human keratinocyte cells by iron doping

J Nanopart Res (2014) 16:2263

Inhibition of the ROS-mediated cytotoxicity and genotoxicity of nano-TiO_2 toward human keratinocyte cells by iron doping

Mara Ghiazza · Elisa Alloa · Simonetta Oliaro-Bosso · Franca Viola · Stefano Livraghi · Diana Rembges · Robin Capomaccio · François Rossi · Jessica Ponti · Ivana Fenoglio

Mara Ghiazza and Elisa Alloa contributed equally to this work.

M. Ghiazza _ S. Livraghi _ I. Fenoglio (&) Dipartimento di Chimica, Interdepartmental Center for Nanostructured Interfaces and Surfaces (NIS)
and ''G. Scansetti'' Interdepartmental Center, University of Torino, Via P. Giuria 7, 10125 Torino, Italy
e-mail: ivana.fenoglio@unito.it

E. Alloa _ D. Rembges _ R. Capomaccio _
F. Rossi _ J. Ponti (&)
European Commission, Joint Research Centre, Institute for Health and Consumer Protection, (EC-JRC-IHCP), Via Fermi 2749, 21027 Ispra, VA, Italy
e-mail: jessica.ponti@jrc.ec.europa.eu

S. Oliaro-Bosso _ F. Viola
Dipartimento di Scienza e Tecnologia del Farmaco, University of Torino, Via P. Giuria 9, 10125 Torino, Italy

Abstract

Nano-TiO_2 powders are widely used in sunscreen lotions as UV filters in combination with other substances. The activation of TiO_2 by UV rays leads to the release of reactive oxygen species (ROS, e.g., hydroxyl radicals and singlet oxygen) which are potentially harmful. For this reason the TiO_2 particles are generally coated with inert materials (e.g., silica or alumina) that inhibit such reactivity. Alternatively, the release of ROS may be inhibited by introducing in the TiO_2 lattice doping elements. In the present study we report a new modification consisting in a wet impregnation of TiO_2 with iron salts followed by a thermal treatment that results in an inhibition of the surface reactivity. The insertion of iron ions also gradually reduces the ability of photo-activated TiO_2 to cleave DNA and proteins. At the same time, a clear inhibition of cyto- and geno-toxicity toward human (HaCaT) keratinocytes was observed. The data presented herein suggest the insertion of Fe^{3+} ions at the surface of nano-TiO_2 as a promising strategy to reduce the photo-induced toxicity of nano-TiO_2 powders.

Keywords Titania _ Iron _ Doping _
Photocatalytic activity _ Genotoxicity _
Keratinocytes _ Health effects

Introduction

Titanium dioxide (TiO_2) is widely used in industry in a wide range of applications. One of the most interesting applications of nano-TiO_2 is as photocatalyst since nano-TiO_2 exhibits a remarkable UV-induced reactivity. When irradiated in wet conditions the generation of different reactive oxygen species (ROS) ($HO^{\bullet}$, $O_2^{\bullet-}$, $^1O_2$, and H_2O_2) is observed(Fujishima et al. 2008). This reactivity is exploited in photocatalysis and in environmental applications like wastewater remediation and manufacturing of self-cleaning tissues and paints (Abidi et al. 2009; Yaghoubi et al. 2010). In contrast, when used as physical blocker of UV radiation in sunscreens (Cosmetics Directive 76/768/EEC, www.fda.gov), this property is undesirable because of the associated potential toxicity of such reactive species (EPA/600/R-09/057F 2010) and because their reactivity toward the organic ingredients in sunscreens included organic filters that are always associated to the inorganic ones (Ricci et al. 2003; Barker and Branch 2008). Therefore, commercial nano-TiO_2 are generally coated with inert materials (Lee et al. 2007; Landsiedel et al. 2010) which inhibits the formation of radical species and singlet oxygen by preventing the contact of the TiO_2 surface with oxygen and water. However, not all the coatings are equally efficient in preventing the release of surface-derived ROS (Sayes et al. 2006; Brezova et al. 2005; Carlotti et al. 2009; Tiano et al. 2010; Buchalska et al. 2010). Antioxidant ingredients are also added to the formula to mitigate the oxidative properties of photogenerated ROS (Carlotti et al. 2009). One possible alternative strategy is to use TiO_2 forms which are less reactive such as rutile.

Doping with metals or nonmetal elements (e.g., nitrogen, carbon, and transition metals) has been shown to be a promising approach to increase the photocatalytic activity of TiO_2 (Carp et al. 2004; Fujishima et al. 2008). As far as metal doping is concerned, photoactivity of transition-metals-doped TiO_2 is a complex function of

i. the dopant concentra-tion; ii. the energy levels of the dopant with respect to the titania valence and conducting band; and iii. its electronic structure and distribution within the TiO_2 lattice. Recently, transition-metals, and particularly iron, rise an increasing interest since they may enhance the photo-efficiency of titania in the visible region; a property very useful in the manufacture of photocatalysts for environmental applications (Fujishima et al. 2008; Elghniji et al. 2012). The photocatalytic efficiency of iron-doped TiO_2 is dependent upon the synthetic routes and the extent of loading. In fact, while an enhancement of the photocatalytic activity is observed for low loadings (Jin et al. 2011; Yu et al. 2010), high loadings may have a detrimental effect (Elghniji et al. 2012; Colmenares et al. 2006; Wen et al. 2012; Yu et al. 2009; Rehman et al. 2009; Fabrega et al. 2010). Manganese has also been proposed to decrease the photoreactivity of TiO_2 (Wakefield et al. 2004).

We recently described a protocol leading to the insertion of iron ions that largely reduce the reactivity and toxicity of a titania specimen (Fenoglio et al. 2013). In the present study a systematic modification of TiO_2 was performed and a series of samples having different iron contents have been prepared and characterized. The ability of the modified powders to generate ROS, to directly damage proteins and DNA, and to induce cell death and genotoxicity on human Keratinocyte HaCaT cells has been evaluated in comparison with the pristine one.

Materials and methods

Titanium dioxide nanoparticles

The rutile–anatase TiO_2 (Aeroxide P25), hereafter named $T_{A/R}$, was purchased from Evonik (Essen, Germany). This sample is obtained by spray pyrolysis and is formed as primary particles of 25 nm which form aggregates of different sizes (mean size 200 nm) (Gerloff et al. 2012).

Preparation of iron-modified samples

Iron was dispersed on the surface of the titania by a wet impregnation method, widely used for the preparation of heterogeneous catalysis (El-Sharkawy et al. 2007). Briefly, 1 g of $T_{A/R}$ was suspended in 3 mL of an aqueous solution of $Fe(NO_3)_3$, at three different concentrations (0.002, 0.02, and 0.2 M). The suspension was dried at 40 °C for 24 h in order to keep in contact the titania support and iron ions. The procedure was carried out a second time. The products obtained ($T_{A/R}$-Fe1, $T_{A/R}$-F2, and $T_{A/R}$-Fe3) were then dried and subsequently calcined at 600 °C for 16 h.

Structural, morphological, and elemental analysis

XRD spectra were collected on a difractometer (PW1830, Phillips) using Co Kα radiation. Diffraction peaks have been indexed according to the ICSD (Inorganic Crystal Structure Database). The crystallites size of the various investigated materials was obtained by employing the Debye–Scherrer equation. Phase composition was obtained via refining with Rietveld method using MAUD (Material Analysis Using

Diffraction, available at http://www.ing.unitn.it/*maud) program (Lutterotti et al. 1997).

The surface areas of powders have been measured by means of BET methods based on N_2 adsorption at 77 K (Micrometrics ASAP 2020). Diffuse Reflectance UV–Visible spectra (DR UV–Vis) were recorded by a Varian Cary 5 spectrometer using a Cary win-UV/scan software. Elemental analysis was performed using an EDAX Eagle III energy-dispersive micro-XRF (μXRF) spectrometer equipped with an Rh X-ray tube and a polycapillary exiting a circular area of nominally 30 μm diameter. Data collection occurred at each point for 200 s detector live time, with X-ray tube settings adjusted for 30 % dead time. Under these experimental conditions about 1×10^6 counts were collected per scan. For each sample, a matrix of at least 10 spots was analyzed.

Optical properties

Diffuse reflectance UV–Vis spectra were recorded by a Varian Cary 5 spectrometer using Cary win-UV/scan software. The value of optical absorption edge Energy (E) was calculated by the Tauc plot of Kubelka–Munk absorption as a function of the photon energy *hv*. (Radecka et al. 2008)

Evaluation of ζ potential

The ζ potential of titania powders was evaluated by means of electrophoretic light scattering (ELS) (Zetasizer Nano-ZS, Malvern Instruments, Worcestershire, UK). The dusts were suspended (50 mg/L) in ultrapure water (Milli-Q) and the f potential was measured after adjusting the pH step by step by the addition of 0.1 M NaOH or 0.1 M HCl

Determination of potentially bioavailable iron

To determine the amount of iron ions which could be extracted from the surface by endogenous chelators, titania samples were incubated in an aqueous solution of ferrozine a strong chelator specific for iron(II) in the presence of ascorbic acid in order to determine the total amount of removable iron. Indeed, ascorbic acid is able to reduce Fe(III) ions to Fe(II) that are then chelated by ferrozine. 20 mg of dust was incubated in 20 mL of a 3 mM solution of ferrozine in the presence of 3 mM ascorbic acid for 5 days. The amount of iron extracted was determined on the supernatant spectrophotometrically (Uvkon 930) by measuring the absorption of the iron–ferrozine complex at 562 nm, following a technique previously described (Lund and Aust 1990; Ghiazza et al. 2011).

Irradiation conditions

In cell-free tests the irradiation experiments were performed with a 500 W mercury/xenon lamp (Oriel Instruments) equipped with an IR water filter to avoid the overheating of the suspensions. Simulated solar light was obtained by applying a 400 nm cut-off filter that let about 5 % of UV light pass in the UVA region. The light irradiance in the UVA region was measured by a Deltahom (Caselle di Selvazzano, Padova, Italy) instrument equipped with a detector operating in the UVA range (315–400 nm). An irradiance of 8.4×10^{-2} W/m^2 was measured in all the experiments. In cellular tests, a tailored UV exposure cabinet equipped with an adjustable ULTRALUX 300 W lamp ensured a homogeneous exposure inside a 6-well plate. The lamp was checked by a Diode Array System for Laboratory measurements (DAYSYLAB SP-J1009, Schreder CMS) (Sacco et al. 2010). The exact exposure position for the 6-well plate has been selected on the basis of UVA/B dose measurements. The applied radiations to the cells in the culture plate were about 0.4 W/m^2 for UVB (280–315 nm) and 2.7 W/m^2 for UVA (315–400 nm). A 3.1 W/m^2 total UVA/B radiation roughly represents the intensity of sunbathing in July/August around noon in central Europe. The exposure duration of 15 min was selected in order to simulate a realistic UV exposure occurring in summer during common daily human activities.

Oxidative damage to DNA

DNA strand breaks

pYES2 plasmid DNA (Invitrogen, Italy) was used as a model. Strand breaks were detected by agarose (1 %) gel electrophoresis. All the experiments were performed with ~ 0.2 mg of powder (pristine and modified) suspended in 30 µL of MilliQ water and then vortexed. To this suspension 3 µL of DNA solution (100– 150 ng/µL) were added and then exposed to a simulated solar light (UV–Vis lamp using a filter having a cut-off of 400 nm) for 10 and 20 min. The control was DNA irradiated for the same time in the absence of any powder in order to exclude a direct damage to this molecule. After irradiation time the suspension was centrifuged and the supernatant was used for gel electrophoresis. DNA bands were stained and visualized with ethidium bromide (Promega, Italy).

*Eco*RI nicking was done with *Eco*RI (20 U/µL) from New England Biolabs, Italy.~ 3 µg of super-coiled plasmid DNA pYES2 were incubated with 50 U of *Eco*RI enzyme in 100 mM Tris–HCl (pH 7.5), 50 mM NaCl, 10 mM $MgCl_2$, and 0.025 % Triton X-100, both in the absence or in the presence of 200 µg/mL ethidium bromide (the final volume of reaction—15 µL). The reaction was carried out at 26 °C for 16 h. 0.5 µL of the sample was loaded on a 1 % (W/V) agarose gel.

Formation of 8-hydroxy-2´deoxyguanosine (8OHdG)

The presence of 8-OHdG produced by oxidative damage of DNA was analysed by a competitive enzyme-linked immunosorbent assay (‘‘Highly Sensitive 8OHdG Check’’ ELISA kit, ListarFish). A DNA extraction Kit (Wizard– SV Genomic DNA Purification System, Promega) was employed for the extraction of DNA from cultured cells (human NCTC purchased by ATCC). DNA samples were incubated with the titania powders and then digested as described below.

10 µg of DNA was exposed in the presence of ~ 0.2 mg of powder (the final volume was made up to 150 µL using MilliQ water) to a simulated solar light (UV–Vis lamp using a filter having a cut-off of 400 nm) for 0, 10, and 20 min. Next, DNA solution were digested sequentially with 6 U of nuclease P1 (ListarFish) in 20 mM sodium acetate pH 5.2 for 1 h at 37 °C, followed by 6 U of alkaline phosphatase (Sigma) in 11 mM Tris–HCl buffer, pH 7.4, for 1 h at 37 °C. The DNA digests were centrifuged at 6,000 ×g for 5’ and 50 µL of the solution (4 µg DNA) were applied to the wells (coated with 8-OdG) of the ELISA kit. The assay was carried out according to the manufacturer’s instructions. Control DNA was processed similarly in the absence of powder. The 8-OHdG monoclonal antibody present in the reagent mixture of the kit reacts competitively with both the 8-OHdG bound to the wells and the 8-OHdG in solution. OD_{450} values read in each well were inversely proportional to the concentration of 8-OHdG in the digested samples of DNA. The results are expressed as 8-OHdG % (mean OD of DNA powder sample × 100/ mean OD of control DNA sample)

Oxidative damage to proteins

Bovine serum albumin (BSA) (Sigma-Aldrich) has been chosen as the model protein. All the experiments were performed with ~5 mg of powder suspended in 50 µL of phosphate buffer 5 mM pH 7.4 and then sonicated for 5 min. To these suspensions, 50 µL of BSA solution (1 mg/mL in phosphate buffer 5 mM pH 7.4) was added and then exposed to a simulated solar light (see ‘‘ Irradiation conditions’’) for 1 h. Then 10 µL of SDS 10 % was added in order to eliminate the adsorbed proteins at the powder surface. After the irradiation, the suspensions were centrifuged (10 min at 10,000 rpm), and the supernatant was boiled at 100 °C in the presence of LAEMMLI solution which is used for SDS-PAGE electrophoresis analysis.

Photogeneration of reactive oxygen species

The generation of radical species was monitored by electron spin resonance (EPR) spectroscopy (Mini-scope 100 EPR spectometer, Magnettech, Germany) using the spin trapping technique using DMPO (5,5-dimethyl-1-pyrroline-*N*-oxide, Alexis Biochem-icals, San Diego, CA) and PBN *(N-tert-butyl-α-*phenylnitrone, Sigma-Aldrich, St. Louis, MO) as spin trapping agents. The generation of $^1O_2$ was monitored by EPR spectroscopy employing 4-oxo-TMP (2,2,6,6-tetramethyl-4-piperidone, Sigma-Aldrich) as a spin probing agent. All the other reagents employed were from Sigma Aldrich. For the aqueous solutions ultrapure Milli-Q water (Millipore, Billerica, MA) was employed. All the tests were performed with an amount of dust corresponding to a surface area of 1.4 m^2.

Superoxide radicals

The powders were suspended in a solution 20 mM PBN in cyclohexane, the suspension was irradiated

with simulated solar light, and constantly stirred. The EPR spectra were recorded on samples suspensions (50 µL) withdrawn after 60 min.

Carboxylate radicals

The powders were suspended in a buffer solution (125 mM potassium phospate buffer pH 7.4) of DMPO (5,5-dimethyl-1-pyrroline-1-oxide, 88 mM) and sodium formate (1 M). The suspension was irradiated with simulated solar light and constantly stirred. The EPR spectra were recorded on a sample suspension (50 µL) withdrawn after 60 min.

Singlet oxygen

The powders were suspended in 1 mL of a solution of 50 mM 4-oxo-TMP (2,2,6,6-tetramethyl-4-piperi-done) in cyclohexane. The suspension was irradiated with simulated solar light and constantly stirred. The EPR spectra were recorded on sample suspension (50 µL) withdrawn after 10 min.

The capability of the dusts to generate singlet oxygen was also monitored by spectrophotometry employing the rubrene as a probe molecule. A 0.15 M solution was prepared by dissolving rubrene in acetonitrile/n-butanol (5:1). The mixture was continuously stirred in the dark to prevent its photoxidation. The amount corresponding to 0.1 m^2 ofexposedsurfaceareaofthedustsweresuspended in 2 mL of the rubrene solution in a quartz vial. The suspension was irradiated with simulated solar light and constantly stirred. After 5 min of incubation the dust was removed by centrifuging the suspension (1200 RCF). The supernatant was filtered through PTFE membrane filters (Advantec, Toyo Roshi Kaisha, Japan; pore diameter 0.20 µm) and the absorbance (λmax = 525 nm) was measured by means of a Uvikon UV–Vis spectrophotom-eter (Kontron Instruments Inc., Everett, MA). A rubrene solution irradiated in the same conditions but in the absence of the dust was employed as blank.

Preparation of nanoparticles suspensions

10 mg of each powder was weighted on an analytical balance and suspended in 1 mL of MilliQ sterile water. Samples were ultrasonicated for 15 min using ultrasonic bath (35 kHz, 320 W; Baldelin, RK100, Germany) and directly diluted in complete cell culture medium (DMEM high glucose (Invitrogen, Italy) added with 10 % (v/v) Fetal Clone II serum (Hyclone, Celbio, Italy) and 1 % (v/v) pen/strep (Invitrogen, Italy) to reach the final testing concentrations of 100 and 500 µg/mL.

Nanoparticles agglomeration on cell media

Nanoparticles size distribution was measured by Differ-ential Centrifugal Sedimentation (DCS) using a sucrose gradient 8–24 % (w/w) (Disc Centrifuge model DC24000, CPS Instruments Europe, The Netherlands) assuming that density of the modified particles were the same as that of the pristine one and automatically detecting the peak of the weight of the particles. The polydispersity index (PdI) was calculated as PdI = - weight mean (Dw)/number mean (Dn). Pristine and modified TiO_2 powders were prepared as described above and diluted in MilliQ water, complete culture medium, and serum-free culture medium reaching the concentration tested of 100 µg/mL. The size has been evaluated in three conditions: at time 0, under irradiation with a Ultralux 300 W lamp installed in an irradiation chamber; and after 2 h of incubation under the standard cell culture conditions (5 % CO_2, 95 % humidity, 37 °C).

Cell culture conditions

Human keratinocyte cells (HaCaT) were originally supplied by the German Cancer Research Center (Germany). The experimental cultures were prepared from deep-frozen stock vials and maintained in culture in a subconfluent state (not more than 70 %). HaCaT cells were cultured in DMEM high glucose 70 (Invitrogen, Italy) mixed with 10 % (v/v) Fetal Clone II serum (Hyclone, Celbio, Italy) and 1 % (v/v) pen/ strep (Invitrogen, Italy), and maintained in the stan-dard conditions (37 °C, 5 % CO_2 and 95 % humidity, Heraeus incubator, Germany).

Cytotoxicity assay

The Colony Forming Efficiency Assay (CFE) was carried out exposing cells to 100 and 500 g/mL of the TiO_2 samples for 2 h under the standard cell culture conditions (5 % CO_2, 95 % humidity, 37 °C) (dark exposure) and for 15 min under UVA/B radiation exposure. HaCaT cells were seeded at a density of 200 cells/dish (60 × 15 mm^2 Petri dish, Corning, Costar, Italy) in 3 mL complete culture medium for dark exposure and at the same density but in 2.5 mL/ well in a 6-well plate (Falcon, Italy) for the under

UVA/B radiation exposure. After 24 h, the medium was changed with the standard complete cell culture medium for the dark condition and with the complete culture medium without Phenol Red for the under UVA/B radiation exposure. Aliquots of the TiO_2 samples suspensions were added to each dish or well obtaining the testing concentrations of 100 and 500 µg/mL. After exposure, the medium was changed with complete fresh culture medium that was renewed twice/week. After 10 days, cells were fixed for 20 min with 3.7 % (v/v) formaldehyde solution (Sigma, Milan, Italy) in Phosphate Buffer Solution(PBS) (19, GIBCO, Italy). Dishes were stained for 30 min with 10 % (v/v) Giemsa solution 95 (GS-500, Sigma, Italy) in ultrapure water. Colonies were scored with GelCount colony counter (Oxford Op-tronix, UK). Each experiment included a negative control (untreated cells); a positive control that induced complete cell death (cells exposed to sodium chromate 1,000 µM, Sigma, Italy); and a control under UVA/B radiation (untreated cell but exposed to UVA/B radiation exposure for 15 min). Results are expressed as CFE (% of the control) for dark exposure or CFE (% of control UVA/B) for radiation exposure. CFE (%) = average of treatment colonies/ average of control colonies × 100. The corresponding standard error mean (SEM) was calculated for at least 3 independent experiments and at least 3 replicates for each experimental point (SEM = SD/ √number of replicates). The statistically significant differences were calculated by the one-way ANOVA analysis (GraphPadPrism4 statistical software, GraphPad Inc., CA, USA).

Genotoxicity assay

For the Comet assay analysis was performed using alkaline protocol and the addition of Fpg and *EndoIII*. 250,000 HaCaT cells were seeded in 3 mL of complete culture medium in each well in 6-well plates (Falcon, Italy). After 24 h, medium was changed with complete cell culture medium for the dark condition and with complete culture medium without phenol red for the UVA/B radiation exposure. Cells were exposed as described for the CFE assay and aliquots of the TiO_2 samples suspensions were added to each well obtaining the testing concentrations of 100 µg/mL. Each experiment included a negative control (untreated cells); a positive control (cells exposed to 100 µM of H_2O_2 Sigma, Italy); and a UVA/B radiation control (cell exposed to UVA/B radiation for 15 min). After exposure, cells were washed twice with 3 mL of PBS, detached with 500 µL/well of trypsin (Invitrogen, Italy) and harvested with 2 mL/well of complete culture medium; cells were counted and 30,000 cells were included in the second layer of each previously prepared slide. The first layer was done by 0.5 % (w/v) normal melting point agarose, the second and third layers were done by 0.5 % (w/v) low melting point agarose (Sigma, Italy). Three slides were prepared for each control and treatment group; one slide was treated with enzyme buffer alone (as a control), the second one was treated with the Escherichia coli Endonuclease III (*Endo*III) enzyme (Tema Ricerca, Italy), and the third one was treated with the E. coli formamidopyrimidine DNA glycosylase (Fpg) enzyme (Tema Ricerca, Italy). After solidification of the agarose, the coverslips were removed and the slides were immersed for 1 h at 4 °C in cold and fresh prepared lysing solution (2.5 M NaCl, 100 mM Na_2EDTA, and 10 mM Tris, pH 10, containing 1 % (v/v) Triton X-100 and 10 % 25 (v/v) dimethylsulfoxide, Sigma-Aldrich, Italy). After lysis, slides were washed with enzyme buffer (100 mM KCl, 10 mM Na_2EDTA, and 10 mM HEPES in MilliQ water for *Endo*III and mixed with 0.1 mg/mL bovine serum albumin for Fpg, both adjusted at pH 7.4) for 15 min at 4 °C and treated with 100 µL of enzyme buffer alone, *Endo*III or Fpg, covered with a coverslip, put in a moist box at 37 °C for 45 min for enzyme buffer alone and *Endo*III enzyme or 30 min for Fpg enzyme. The slides were placed in a horizontal gel electrophoresis tank filled with electrophoresis cold buffer (0.3 M NaOH and 1 mM Na_2EDTA) for 40 min. Electrophoresis was then carried out at 25 V and 300 mA for 30 min at 4 °C. After the electrophoresis, the slides were washed twice for 5 min with neutralizing buffer (0.4 M Tris, pH 7.5), fixed with absolute ethanol (Carlo-Erba, Italy) for 3 min, and stained with 50 µL 40 ethidium bromide (0.4 M/mL; Sigma-Aldrich) before the analysis. Analysis was made using the Komet 6 Image Analysis System (Kinetic Imaging Ltd, Liverpool, UK) fitted with fluorescence microscope (Olympus, Italy) with the following settings: magnification 409, wide band excitation filter 480–550 nm, and barrier filter 590 nm. Data are expressed as median of DNA (% in Tail) of at least three experiments (100 cells per run) and the statistically significant difference of the treatment versus the corresponding controls was calculated by the one-way ANOVA analysis (GraphPadPrism4 sta-tistical software, GraphPad Inc., CA, USA).

Results

Structural properties of the powders and elemental composition

A commercial sample composed by anatase and rutile phases (Aeroxide P25) was chosen as starting materials due to its high photoactivity and widespread use. On the other hand, powders having a similar proportion of anatase and rutile were reported to be contained in the core of commercial TiO_2 powders used as ingredients in sunscreens (Bolis et al. 2012). Iron ions were inserted by a wet impregnation method followed by calcination at 600 °C. The elemental composition of the modified powders, evaluated by XRF spectroscopy, is reported in Table 1. The amount of iron changed by increasing the concentration of iron salt in the solution used for the impregnation and varied from 0.07 % w/w for $T_{A/R}$-Fe1 to 4.3 % w/w for $T_{A/R}$-Fe3. Since the thermal treatment may cause the conversion of the anatase phase to the more thermodynamic stable rutile the abundance of crys-talline phases were evaluated by Rietveld refinement method (Table 1) (Lutterotti et al. 1997). The pristine sample showed a rutile/anatase ratio of 12.7. Significant changes in the crystalline phases ratio has been observed following the thermal treatment. As expected, the relative amount of rutile increases in all the samples. Reduction of the specific surface area (SSA) of the powder was also observed probably because of an increase of the crystallite size during heating (Table 1). However, the anatase to rutile phase transition and SSA reduction were gradually inhibited by increasing the amount of iron ions. The XRD analysis of $T_{A/R}$-Fe3 revealed an additional diffraction peak typical of hematite (a-Fe_2O_3) (Fig. 1). The optical adsorption properties of pristine TiO_2 and Fe-TiO_2 material were examined with UV–Vis diffuse reflectance spectroscopy. The diffuse reflectance spectra expressed in terms of Kubelka–Munk equivalent absorption units are presented in Fig. 2. For the pristine TiO_2, the typical absorption edge around 387 nm due to the intrinsic band gap excitation of anatase (3.2 eV) is clearly visible. Pristine TiO_2 has no absorption in the visible region (>400 nm), whereas Fe-TiO_2 materials show significant enhancement in the 400–600 nm region (Fig. 2A). Such absorption increases with increasing the iron loading and it is accompanied by color changes from white to pale yellow (Inset in Fig. 2A) for samples $T_{A/R}$-Fe1 and $T_{A/R}$-Fe2. Considering that no trace of segregated iron oxide was detected by XRD analysis in these two samples, such change in visible light absorption can be ascribed to the insertion of iron in the TiO_2 lattice (Elghniji et al. 2012). The spectrum of $T_{A/R}$-Fe3 is more complex and characterized by a step-like adsorption (at about 600 nm) indicating the overwhelming presence of iron oxide (Fe_2O_3) particles, as already revealed by XRD spectrum and the color of the samples which turns to reddish (inset in Fig. 2A) (Pal et al. 1999).

The value of optical absorption edge Energy (E), calculated from the Tauc plot of Kubelka–Munk absorption, as a function of the photon energy hm (Radecka et al. 2008) are reported in Fig. 2B.

Such method can be also applied to estimate the Band Gap energy edge (Eg) in semiconducting oxide provided that the absorption curve is not affected by further absorption due to additional electronic transition or additional component of the system. This condition is satisfied for $T_{A/R}$, $T_{A/R}$-Fe1, and $T_{A/R}$-Fe2 samples while in the case of $T_{A/R}$-Fe3 the presence of Fe_2O_3 strongly affects the absorption edge and, therefore, the Band Gap energy cannot be evaluated. No significant change in Eg value was observed for $T_{A/R}$-Fe1 (2.98 eV) with respect to the pristine sample (3.00 eV) whereas in the case of $T_{A/R}$-Fe2 sample a red-shift of about 0.2 eV was observed.

Characterization of the surface of TiO_2

Biofluids are rich in molecules which may act as chelators and mobilize iron ions weakly adsorbed at the surface. Mobilized ions, being redox-active, may induce oxidative stress e.g., by generating free radicals through Fenton reaction (Fenoglio et al. 2011). To investigate the possible occurrence of such a process the powders were incubated with a solution of a chelator having high affinity for Fe^{2+} ions (Ferrozine) alone or in combination with a reducing agent (ascorbic acid) according to a method previously described (Lund and Aust 1990; Ghiazza et al. 2011). The amount of iron ions extracted in this condition was lower than 15 % of the total amount for all the Fe-doped titania suggesting that iron ions were strongly coordinated at the surface or migrate in the sublayer of the particles. Fe^{3+} ions have, in fact, a ionic radius similar to Ti^{4+} and may, therefore, substitute them in the lattice (Elghniji et al. 2012). As expected, the amount of removable iron slightly increased by increasing the loading.

Table 1 Physicochemical properties of the TiO_2 samples

Sample	Crystalline phase (% wt)	Iron content (% wt Fe)	Specific surface area (m^2/g)	Crystallite size (nm)	ζ potential water, pH 7.4	Potentially bioavailable iron (% wt Fe)
$T_{A/R}$	Anatase 88.7, rutile 11.3	<0.01	52.6	Anatase 25 ± 3, rutile 45 ± 7	-21.5	<0.01
$T_{A/R}$-Fe1	Anatase 58.1, rutile 41.9	0.07	30.9	Anatase 29 ± 1, rutile 61 ± 3	-38.3	<0.01
$T_{A/R}$-Fe2	Anatase 79.1, rutile 20.9	0.45	42.4	Anatase 26 ± 3, rutile 62 ± 8	-37.8	0.01
$T_{A/R}$-Fe3	Anatase 76.7, rutile 20.6 ematite 2.7	4.3	38.8	Anatase 25 ± 2, rutile 41 ± 3	-36.5	0.02

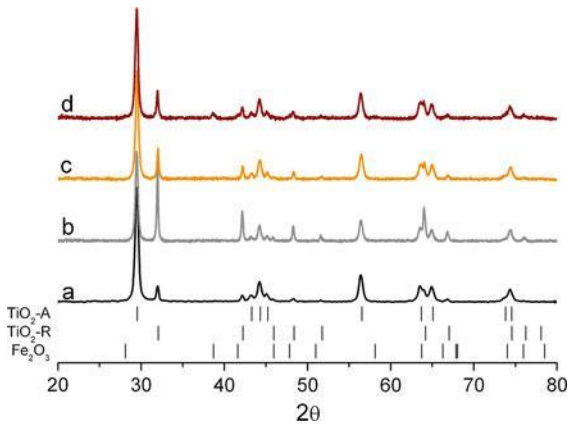

Fig. 1 XRD patterns of a $T_{A/R}$; b $T_{A/R}$-Fe1; c $T_{A/R}$-Fe2; and d $T_{A/R}$-Fe3. The main diffraction picks of the detected crystalline phases are indicated: TiO_2-A: anatase polymorph (ICSD 01-073-1764); TiO_2-R: rutile polymorph (ICSD 00-065-0192); and Fe_2O_3: hematite (ICSD 01-084-0306)

In aqueous solutions, the surface of TiO_2 may exhibit the positive or negative charges depending upon the pH. In fact, the hydroxyls (Ti–OH) exposed at the surface have an acidic behavior and are dissociated at high pH ($Ti–O^-$). At low pH surface Ti^{4+} species prevail imparting to the surface a positive charge. The extent of the surface charge may be estimated by measuring the f potential in water, i.e., the potential measured across the double layer of ions around the particles (Fenoglio et al. 2011). In Fig. 3 the ζ potential curves as a function of pH of the pristine and modified powders are reported.

The introduction of iron ions at the surface of TiO_2 shifted the f potential curves and the PZC toward lower pH values (Fig. 3 and Table 1) suggesting a higher Brønsted acidity of the surface of the modified samples. A similar behavior was observed by other Authors for other forms of iron-doped titania (El-Sharkawy et al. 2007; George et al. 2011). For the $T_{A/R}$-Fe3 a lower shift of the curve was observed probably due to an additional effect of hematite. Hematite shows, in fact, a ζ potential curve shifted toward higher pH (Fig. 3).

Photo-induced generation of reactive oxygen species

The photocatalytic efficiency of TiO_2 is generally evaluated in photocatalysis by measuring the extent of degradation of organic molecules or dyes. These methods are, however, not fully predictive of the ability of TiO_2 to induce oxidative stress to cells because of the different chemical natures of the probe with respect to biomolecules. Here, to gain a complete picture of the processes which may occur at the surface of TiO_2 nanoparticles in a biological environment the ability to generate primary ROS ($HO^\bullet$, $O_2^{\bullet-}$, $^1O_2$), evaluated by EPR/spin trapping/probing techniques, has been integrated with experiments apt to evaluate the ability to induce oxidative damage to biomolecules according to a protocol previously reported (Corazzari et al. 2012; Ghiazza et al. 2013). Simulated solar light was used to activate the powders.

Reductive (e^-) activity of irradiated iron-modified TiO_2

Photogenerated electrons may reduce oxygen to superoxide radicals anions following reaction (1).

$$e^- + O_2 \rightarrow O_2^{\bullet -} \quad (1)$$

Superoxide radicals anions can be detected both as absorbed species on TiO_2 (Fenoglio et al. 2009) or as released species in solution. In the second case they have a short lifetime and need to be trapped by a spin trap molecule, or to react with a spin probe, to be detected by EPR. By irradiating with the simulated solar light the pristine powder suspended in a solution of the spin trap N-tert-butyl-a-phenylnitrone (PBN), a broad three-line spectrum was observed (Fig. 4A spectrum a) accordingly to what was previously

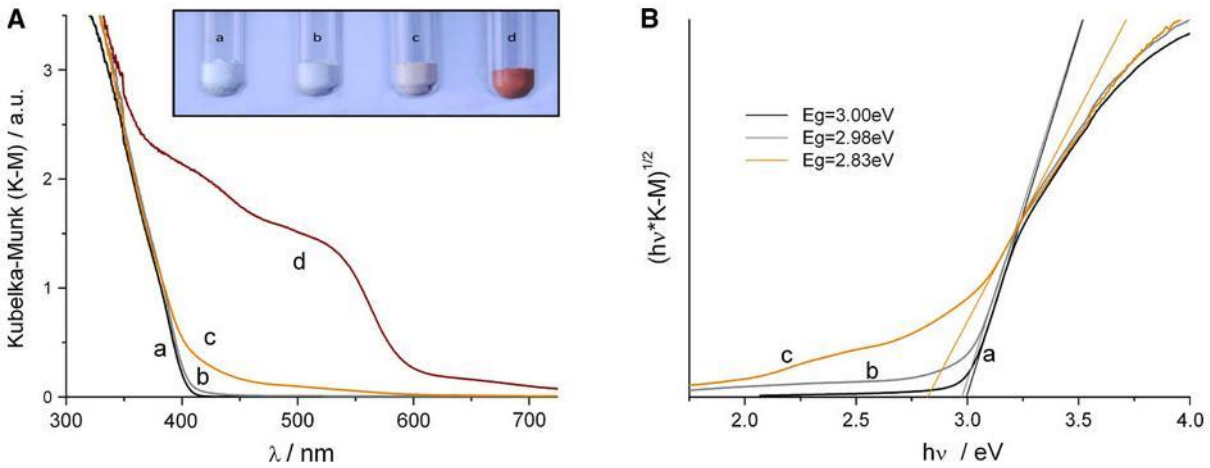

Fig. 2 Optical properties of the TiO_2 samples. A UV/Vis reflectance of the titania samples, in the inset the color of the powders; B Tauc plot of Kubelka–Munk absorption as a function of the photon energy; a $T_{A/R}$; b $T_{A/R}$-Fe1; c $T_{A/R}$-Fe2; and d $T_{A/R}$-Fe3

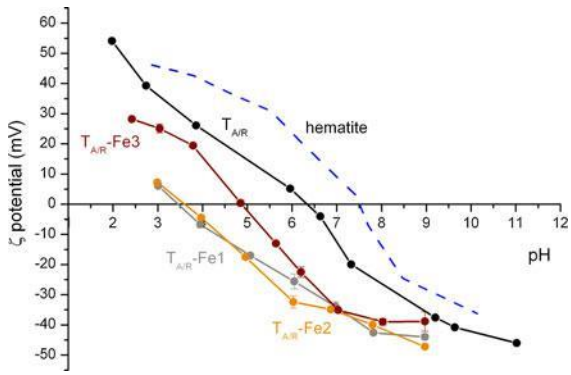

Fig. 3 ζ Potential curves as a function of pH of the TiO_2 sample. The ζ potential of a sample of hematite is reported for comparison

reported by some of us (Corazzari et al. 2012). A signal of similar intensity was observed for $T_{A/R}$-Fe1 (Fig. 4A spectrum b). Conversely, on the powders with medium and high amount of iron ($T_{A/R}$-Fe2 and $T_{A/R}$-Fe3) no signal corresponding to superoxide free radicals has been detected suggesting a full inhibition of the ability of TiO_2 to reduce oxygen under solar light irradiation (Fig. 4A spectra c, d).

Oxidative (h^+) activity of irradiated iron-modified TiO_2

Photogenerated holes may react both with water leading to the generation of hydroxyl radicals (2) and with organic molecules (e.g., sodium formate) generating carbon-centered radicals following reaction (3):

$$h^+ + OH^- \rightarrow {}^{\bullet}OH \quad (2)$$

$$h^+ + HCO_2^- \rightarrow CO_2^{\bullet -} + H^{+:} \quad (3)$$

Under irradiation with simulated solar light in the presence of sodium formate and 5,5-dimethyl-1-pyrroline-*N*-oxide (DMPO) as a spin trap molecule, a strong six-line signal typical of the DMPO-$CO_2^{\bullet -}$ adduct was observed for pristine powder (Fig. 4B, spectrum a). A signal of lower intensity was observed for $T_{A/R}$-Fe1 and $T_{A/R}$-Fe2 (Fig. 4B) while the oxidative activity was almost completely suppressed for the $T_{A/R}$-Fe3 sample (spectrum d).

Generation of singlet oxygen

Singlet oxygen ($^1O_2$) was reported to be generated upon irradiation of TiO_2 (Buchalska et al. 2010; Fenoglio et al. 2013). Being diamagnetic, this species is not detected by EPR. However, $^1O_2$ may react with the spin probe 4-oxo-TMP to give a nitroxide radical as previously reported by other authors (Konaka et al. 1999; Brezova et al. 2005). By irradiation of the pristine powder in the presence of spin probe, a three-line signal typical of the nitroxide radical was obtained (Fig. 4C, spectrum a). Oppositely, no signal was obtained by irradiating the Fe-doped powders (Fig. 4C, spectra b–d). To confirm the results, the generation of singlet oxygen was further evaluated spectrophotometrically using a colored dienic

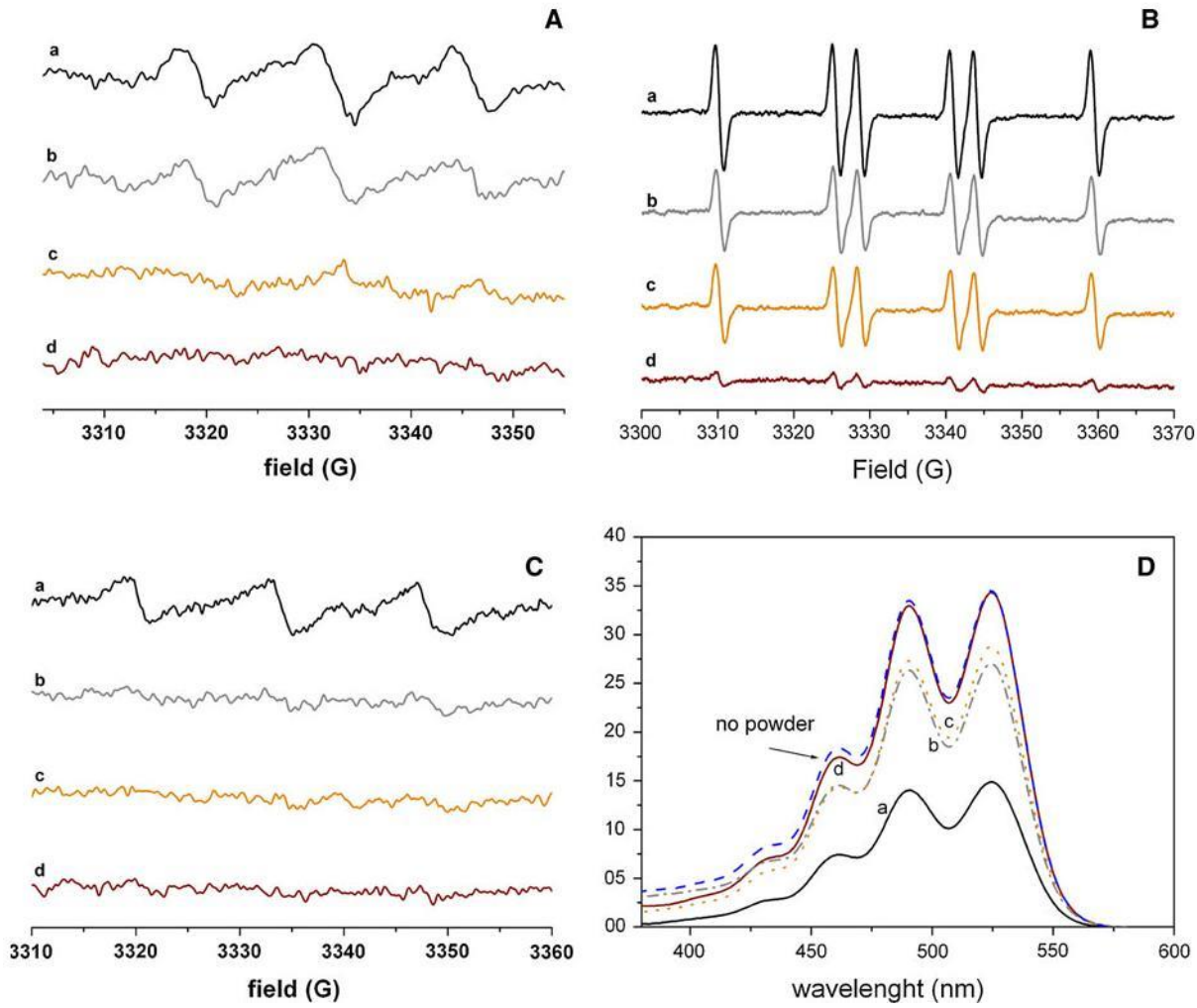

Fig. 4 Generation of reactive oxygen species by the TiO_2 samples under simulated solar light conditions. Generation of ROS detected by EPR/spin trapping or probing techniques: A superoxide radicals ($O_2^{\bullet-}$); B carboxylate radicals ($CO_2^{\bullet-}$); C singlet oxygen ($^1O_2$); and D generation of singlet oxygen ($^1O_2$) under simulated solar light conditions detected spectrophotometrically using rubrene as the probe. a $T_{A/R}$; b $T_{A/R}$-Fe1; c $T_{A/R}$-Fe2; d $T_{A/R}$-Fe3

molecule (rubrene) as the probe. Singlet oxygen specifically reacts with the orange rubrene by a [4 + 2] cyloaddition producing a colorless endoperoxide (Clennan and Pace 2005; Kim et al. 2009). The amount of singlet oxygen generated is thus inversely proportional to the absorbance measured on the supernatant of the solution after contact with TiO_2 (Fig. 4D). Also, in this case, the pristine titania resulted to be the most active while the high Fe-doped TiO_2 ($T_{A/R}$-Fe3) resulted to be the less active in generating singlet oxygen, as revealed by the absorbance values in Fig. 4D, spectra b and e, respectively. The other two Fe-doped samples (spectra c and d) slightly decreased the absorbance of probe molecule (rubrene) suggesting a negligible generation of singlet oxygen.

Photo-induced damage to biomolecules

Cellular biomolecules have a specific role in cells. If they are damaged their function may change leading to cell death or accelerating aging. Biomolecules damage is usually ascribed to an oxidation process following the reactions between ROS and molecules. TiO_2 is known to generate high amount of ROS under UV light and thus may damage biomolecules such as

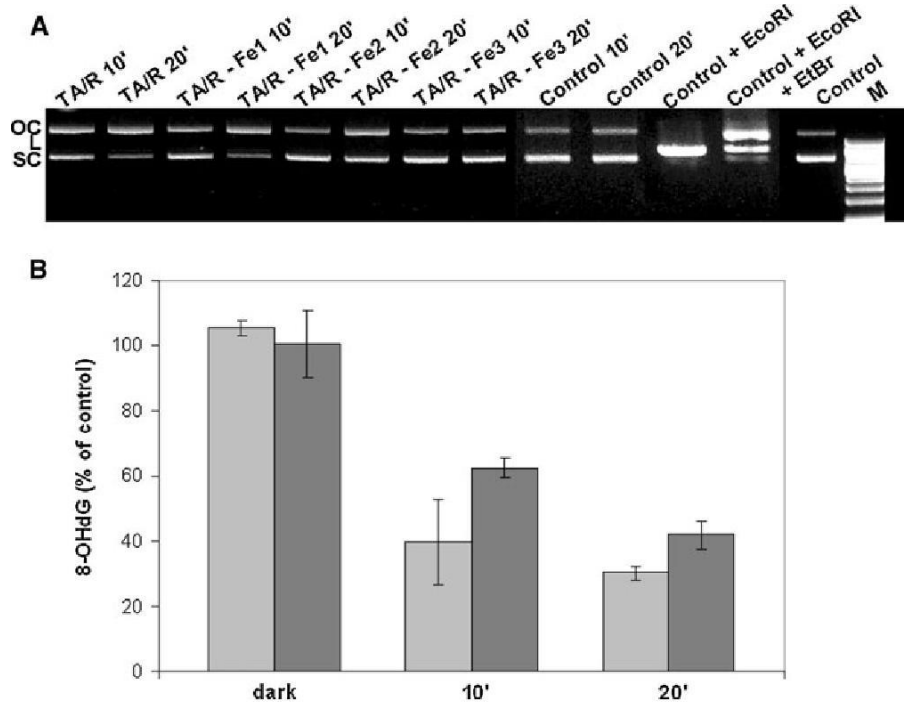

Fig. 5 A Photo-induced damage to double-stranded supercoiled plasmid DNA. The DNA was irradiated for 10 and 20 min in the absence (control) and in the presence of the TiO_2 samples. M marker. B Photo-induced generation of 8-OHdG. Light gray DNA+$T_{A/R}$ and dark gray DNA+$T_{A/R}$-Fe3, under sunlight simulator (0, 10, and 20 min)

lipids, proteins, and DNA. The oxidative damage, under illumination with simulated solar light, to DNA and protein is documented in Figs. 5 and 6, respec-tively. DNA damage was studied by agarose gel electrophoresis of a plasmid DNA after irradiation for 10 and 20 min in the presence of TiO_2 powders. The induction of DNA strand breaks was evaluated by the conversion of supercoiled plasmid double-stranded DNA (SC) to open circular (OC) and linear forms (L) (Fig. 5A). The controls of open circular and linear forms were obtained by incubating the plasmid DNA with *Eco*RI, both in the absence or in the presence of a high concentration of ethidium bromide (Pfannsch-midt and Langowski 1998) that partially inhibits the DNA cutting by EcoRI, causing the formation of nicked DNA (OC). The irradiation for 10 and 20 min of plasmidic DNA incubated with the $T_{A/R}$ powder caused a significant increase of OC form, with respect to plasmidic DNA not irradiated or irradiated for the same time in the absence of powder.

Damage caused by Fe-doped TiO_2 decreased by increasing the amount of iron. Low doped titania behaved similar to the undoped titania generating mainly open circular DNA, while the other two Fe-doped samples caused less ($T_{A/R}$-Fe2) or no damage ($T_{A/R}$-Fe3).

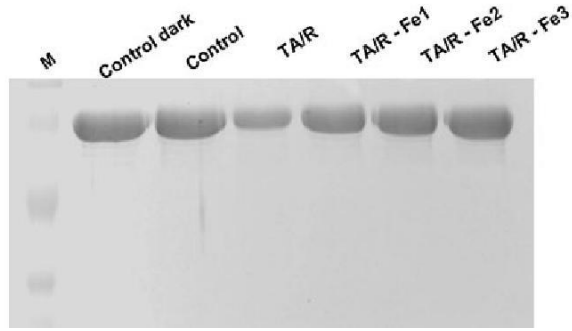

Fig. 6 Photo-induced damage to proteins. Bovine serum albumin (BSA) was used as model protein. Control: BSA, *M* marker

The occurrence of DNA strand breaks is indicative of high capacity of the tested substance to induce DNA oxidation. However, oxidation of nucleobasis may also occur in the absence of any evident cleavage of DNA. For this reason the less reactive powder $T_{A/R}$-Fe3 was also tested in an ELISA competitive assay for its ability to induce the formation of 8-hydroxy-deoxyguanosine, which is a widely used marker of DNA damage (Fig. 5B). Albeit at a less extent than the pristine TiO_2 the modified sample still retains the ability to induce the oxidation of guanosine.

Table 2 Mean particle size distribution of the TiO_2 samples in water, HaCaT cell culture medium without and with 10 % (v/v) serum

Sample	Mean size in water (nm/PdI)			Mean size in serum-free cell medium (nm/PdI)			Mean size in cell medium (nm/PdI)		
	Time 0	15-min UV irradiation	2-h dark	Time 0	15-min UV irradiation	2-h dark	Time 0	15-min UV irradiation	2-h dark
$T_{A/R}$	89/1.60	119/1.70	104/3.44	245/2.12	471/6.6	310/2.05	178/3.5	343/1.52	184/4.25
$T_{A/R}$-Fe1	ND	ND	ND	ND	ND	ND	ND	ND	ND
$T_{A/R}$-Fe2	203/4.45	164/1.27	202/2.49	303/2.15	646/9.78	368/2.56	148/2.47	278/3.03	130/2.63
$T_{A/R}$-Fe3	108/1.64	130/1.52	105/2.44	252/1.68	747/10.03	320/2.09	247/2.79	320/2.02	190/3.48

Samples were measured by CPS at time 0 and after 15 min of exposure to UVA/UVB irradiation or 2 h of incubation in the cell culture incubator (dark)

ND not determined

The protein damage was tested on bovine serum albumin (BSA) by irradiating a mixture of TiO_2 and BSA for 1 h and analyzing the supernatant by SDS-Page electrophoresis (Fig. 6). Simulated solar light did not cause any damage to BSA alone. Addition of the undoped TiO_2 decreased the intensity of the band corresponding to the BSA (90 kDa), indicating BSA damage (Fig. 6, lane 3). The intensity of the band was restored in the presence of Fe-doped TiO_2 powders containing increasing amounts of iron at the surface of titania.

Aggregation in cell culture

For a proper biological hazard assessment, dispersion in culture medium has to be carefully monitored (Magdolenova et al. 2012). Here, size distribution of aggregates was measured by centrifugal sedimentation in the different testing conditions adopted for the biological tests. As expected, the powders appeared highly polydispersed in any condition as suggested by the high PdI values. In water, the particles size of TiO_2-Fe2 was higher than the pristine one suggesting a high degree of agglomeration likely due to a lower electrostatic repulsion among aggregates with respect to the pristine sample. In cell media an increase of the particles size was observed for all the samples likely due to the high ionic strength of the solution. On the other hand, the addition of proteins causes a decrease of the particles size with respect to the serum-free cell media following the adsorption of proteins at the surface. It is noteworthy that irradiation always caused an increase of the particle size. The suspension of the powders in cell media appeared stabile up to 2 h (Table 2).

Effect of the TiO_2 samples on the colony forming efficiency of HaCaT cells

$T_{A/R}$-Fe2 and $T_{A/R}$-Fe3 were selected to be tested for their cytotoxic potential on HaCaT cell line using the CFE assay in the dark (Fig. 7A) and under UVA/UVB exposure (Fig. 7B) in comparison with the pristine sample ($T_{A/R}$). Results did not show any statistically significant toxicity induced by all the TiO_2 NPs tested in the dark. Oppositely, statistically significant toxicity was observed for $T_{A/R}$ and $T_{A/R}$-Fe2 tested under sunlight irradiation (Fig. 7B), while in the same experimental conditions no toxicity was observed for $T_{A/R}$-Fe3.

Genotoxicity of the TiO_2 samples

To evaluate the capacity of the powders to induce genotoxic effects the alkaline comet assay protocol modified with the use of Fpg and *Endo*III enzymes was used. While the *Endo*III enzyme principally detects the oxidative damage of pyrimidines, the Fpg enzyme especially acts on the oxidized purinic sites as the 8-oxo-G (Collins et al. 2000).

The experiments were carried out under the standard cell culture conditions (dark), in parallel with simulated sunlight radiation exposure and cells exposed to 100 μg/mL of each sample. The effect of the powders in the dark was not statistically significant with respect to the negative control (Fig. 8A).

The damage observed after UVA/B radiation exposure in the presence of pristine powder was highly statistically significant, whereas no significant effects were detected in the presence of $T_{A/R}$-Fe2 and $T_{A/R}$-Fe3 (Fig. 8B) although a slight toxicity was observed after HaCaT exposure to $T_{A/R}$-Fe2 under UV conditions (Fig. 7B). However, a small increase of the amount of oxidized purines was detected for both the modified samples.

Discussion

Iron is generally associated to an increase of the surface reactivity, and hence toxicity of particulates (Kagan et al. 2006; Pulskamp et al. 2007; Turci et al. 2011; Ghiazza et al. 2011). Having a standard redox potential in water E° = 0.77 V, iron ions may catalyze the formation of ROS, e.g., by generating hydroxyl radicals through reaction with hydrogen peroxide (Fenton reaction), which may in turn induce oxidative stress. This may occur not only if the ions are mobilized in biofluids but also if they are bound to the surface of particles (Shoonen et al. 2006; Fenoglio et al. 2011). The association of iron to TiO_2 nanoparticles is a peculiar case. In fact, it has been reported to both enhance electron/hole separation; thus, increasing the photocatalytic activity or increasing the rate of recombination of the charge carriers leading to a detrimental effect. The concentration of Fe^{3+} ions has been shown to be a key factor since low loading increases the efficiency (Jin et al. 2011; Yu et al. 2010) while an high loading has generally the opposite effect (Elghniji et al. 2012; Colmenares et al. 2006; Wen et al. 2012; Yu et al. 2009; Rehman et al. 2009;

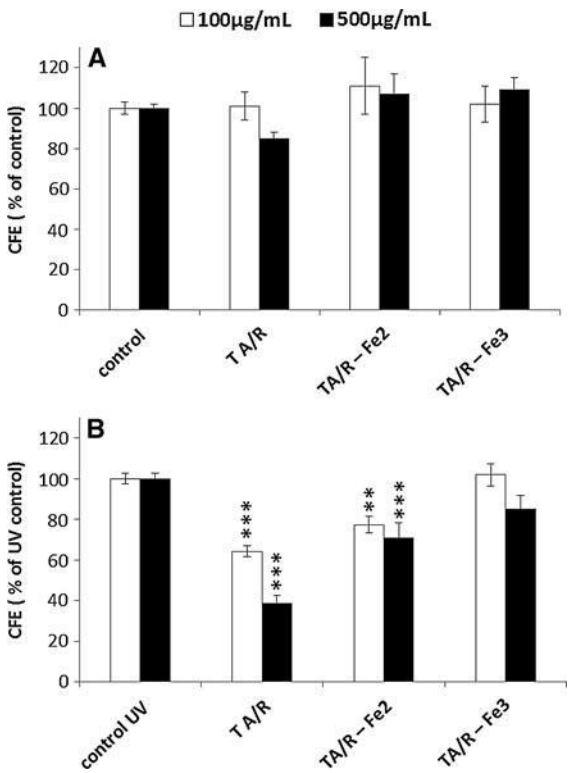

Fig. 7 Effect of the TiO_2 samples on the colony forming efficiency (CFE) on HaCaT cells exposed to 100 and 500 µg/mL of TiO_2 samples. **A** 15 min under UVA/B radiation exposure and **B** 2 h of exposure, under standard cell culture conditions. Results are expressed as CFE % of the negative control (**A**) and CFE % of control UV (**B**). ***P <0.001; **P <0.01

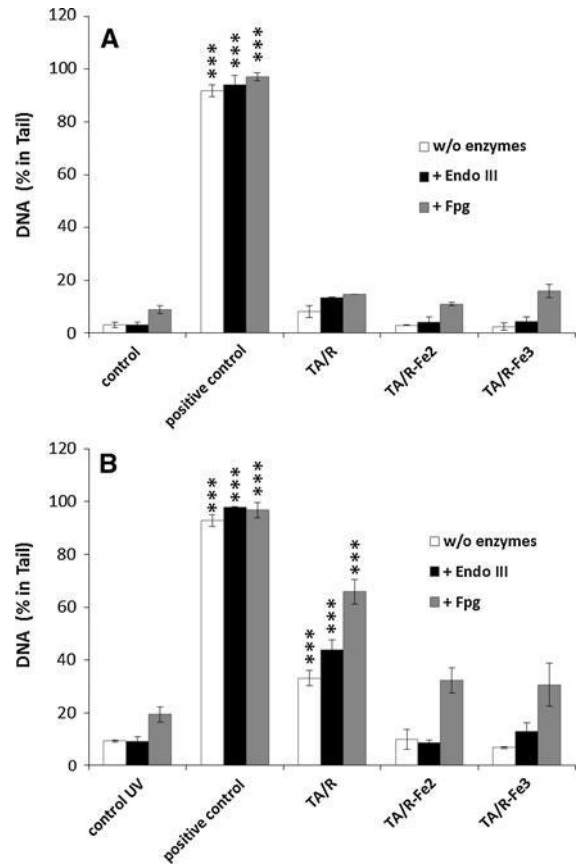

Fig. 8 Primary DNA damage (w/o enzymes), oxidative pyrimidines (+*Endo*III), and purine (+Fpg) DNA damage, measured by Comet assay in HaCaT cells after exposure to 100 µg/mL of TiO_2 samples, under the standard cell culture conditions, 2 h of exposure (**A**) and under simulated solar light, 15 min of exposure (**B**). Results are expressed as % of DNA in tail. ***P < 0.001

Fabrega et al. 2010). A large variability in the photo-efficiency of iron-loaded titania specimens is found in the different studies, likely due to the different methods of doping used.

Here, a wet impregnation protocol leading a relatively high amount of iron to be associated to the nanoparticles has been used. A reduction of both oxidative and reductive photoreactivity was found for the two modified sample $T_{A/R}$-Fe2 and $T_{A/R}$-Fe3 (Fig. 4). The effect was more pronounced on the generation of superoxide and singlet oxygen that were suppressed already in the $T_{A/R}$-Fe2, while the reactivity toward sodium formiate was significantly decreased only for the high loaded sample. The data obtained herein are apparently in contrast with those obtained by George et al. (2011). In this study, a series of iron-doped TiO_2 (Fe 0–10 %) was synthesized and tested for their photocatalytic activity and phototoxicity toward a macrophage cell line. The Authors observed a clear reduction of the band gap energy by increasing the iron content which correlated with an increased oxidant reactivity and phototoxicity. The contrasting results may be explained by the different method of synthesis: the doped titania was obtained by George et al. by flame spray pyrolysis while in the present case a wet impregnation method was used to modify the surface of commercial rutile/anatase sample (Aeroxide P25). While in the previous work homogeneous dispersion of iron inside the titania framework was obtained (George et al. 2011), the method used herein lead to the grafting of iron ions at the surface. During the thermal treatment ions likely migrate in the sublayers of the particles as suggested by the low amount of ions which may be extracted by chelators, by the observed narrowing of the band gap (almost in $T_{A/R}$-Fe2 sample) and by the inhibitory effect of doping on the anatase/rutile transition (see hereafter).

The inhibitory effect of iron was confirmed by the observed reduction of the reactivity toward proteins (Fig. 6) and DNA (Fig. 5A). It is noteworthy, however, that the high loaded sample still retains the ability to oxidize the nucleobases, albeit at a minor extent than the pristine powder. This may be related to the residual oxidative activity of this sample (Fig. 5B).

The treatments performed also lead to a reduction of the surface area and an increase of the abundance of the more stable and less photoreactive phase, rutile. Both the parameters may account for the observed reduced photo-induced reactivity. However, by increasing the abundance of iron ions, the conversion of the anatase to rutile and the reduction of the surface area were inhibited. This effect was probably due to a perturbation of the lattice structure by Fe^{3+} ions that, having an ionic radius similar to Ti^{4+}, may substitute them in the first sublayers of the particles. Since the decrease in surface reactivity has an opposite trend with respect to the abundance of rutile the effect appears to be related to iron insertion.

The ability of TiO_2 nanoparticles to induce inhibition of cell viability as well as DNA damage under UV exposure is well documented (Xue et al. 2010; Park et al. 2011; Shukla et al. 2011; Sanders et al. 2012; Jaeger et al. 2012; Fenoglio et al. 2013). These effects are strictly related to the photogeneration of ROS by TiO_2 nanoparticles and, in particular, to the ability to generate singlet oxygen (Fenoglio et al. 2013). The two powders having the lower surface reactivity ($T_{A/R}$-Fe2 and $T_{A/R}$-Fe3) were tested for their effect on the viability and for genotoxicity on human keratinocytes in comparison with the pristine one. The pristine powder was found to induce both cytotoxicity (Fig. 7B) and genotoxicity (Fig. 8B) to human kerat-inocytes when activated with UVA/B radiation while no effect was observed in the dark (Figs. 7A, 8A).

A reduction of both cytotoxicity and genotoxicity was observed for the iron-doped samples which was dependent upon the amount of iron introduced. Note, however, that a small increase of the amount of oxidized purines was observed even for the high loaded modified samples. This correlates well to the observed capacity of the $T_{A/R}$-Fe3 to induce the oxidation of guanine nucleotide base to 8OHdG on plasmidic DNA after increasing irradiation times. The ability of $T_{A/R}$-Fe3 to contrast the oxidative damage to purines was less significant in the ELISA test than in the Comet assay, possibly due to a different estimation of the overall amount of 8OHdG after DNA hydrolysis in the two test. In fact, in the Comet assay, if several nucleobases are oxidized in close proximity, the lesion recognized by Fpg will behave as a single DNA strand (Gedik et al. 2002). The ability of the whole cells to repair single-strand breaks (SSB) damage should also be considered.

Taken together, these results suggest that the doping method described here largely inhibits, albeit does not totally suppress, the ability of TiO_2 to induce DNA damage.

In conclusion, the data reported herein show that impregnation with iron salts may be a promising strategy to reduce the cytotoxicity and genotoxicity toward keratinocytes of nano-TiO_2 to be used as UV filters.

Acknowledgment This research has been carried out with the financial support of the University of Torino (Progetti di Ricerca finanziati ex 60 %- 2012) project title: ''Integrated chemical tests for the evaluation of the oxidative potential of nanopowders'' and by Regione Piemonte (Progetti di Ricerca Sanitaria Finalizzata 2009, project title ''Inattivazione di polveri nanometriche di TiO_2 per la prevenzione di patologie legate alla loro esposizione lavorativa ed ambientale''). This work was also supported by the Work program Action 15024: Nanobiotechnologies of DG Joint Research Centre.

References

Abidi N, Cabrales L, Hequet E (2009) Functionalization of a cotton fabric surface with titania nanosols: applications for self-cleaning and UV-protection properties. ACS Appl Mater Interface 1:2141–2146. doi: 10.1021/am900315t

Barker PJ, Branch A (2008) The interaction of modern sun-screen formulations with surface coatings. Prog Org Coat 62:313–320. doi: 10.1016/j.porgcoat.2008.01.008

Bolis V, Busco C, Ciarletta M, Distasi C, Erriquez J, Fenoglio I, Livraghi S, Morel S (2012) Hydrophilic/hydrophobic fea-tures of TiO_2 nanoparticles as a function of crystal phase, surface area and coating, in relation to their potential tox-icity in peripheral nervous system. J Colloid Interface Sci 369:28–39

Brezova V, Gabcova S, Dvoranova D, Stasko A (2005) Reactive oxygen species produced upon photoexcitation of sunsc-reens containing titanium dioxide (an EPR study). J Pho-tochem Photobiol B-Biol 79:121–134. doi: 10.1016/j. jphotobiol.2004.12.006

Buchalska M, Kras G, Oszajca M, Lasocha W, Macyk W (2010) Singlet oxygen generation in the presence of titanium dioxide materials used as sunscreens in suntan lotions. J Photochem Photobiol A Chem 213:158–163. doi: 10. 1016/j.jphotochem.2010.05.019

Carlotti ME, Ugazio E, Sapino S, Fenoglio I, Greco G, Fubini B (2009) Role of particle coating in controlling skin damage photoinduced by titania nanoparticles. Free Radic Res 43:312–322. doi: 10.1080/10715760802716633

Carp O, Huisman CL, Reller A (2004) Photoinduced reactivity of titanium dioxide. Prog Solid State Chem 32:33–177. doi: 10.1016/j.progsolidstchem.2004.08.001

Clennan EL, Pace A (2005) Advances in singlet oxygen chemistry. Tetrahedron 61:6665–6691. doi: 10.1016/j.tet.2005.04.017

Collins PG, Bradley K, Ishigami M, Zettl A (2000) Extreme oxygen sensitivity of electronic properties of carbon nanotubes. Science 287:1801–1804. doi: 10.1126/science.287.5459.1801

Colmenares JC, Aramendia MA, Marinas A, Marinas JM, Urbano FJ (2006) Synthesis, characterization and photo-catalytic activity of different metal-doped titania systems. Appl Catal A Gen 306:120–127. doi: 10.1016/j.apcata.2006.03.046

Corazzari I, Livraghi S, Ferrero S, Giamello E, Fubini B, Fenoglio I (2012) Inactivation of TiO_2 nano-powders for the preparation of photo-stable sunscreens via carbon-based surface modification. J Mater Chem 22:19105–19112. doi: 10.1039/c2jm32876c

Elghniji K, Atyaoui A, Livraghi S, Bousselmi L, Giamello E, Ksibi M (2012) Synthesis and characterization of Fe^{3+} doped TiO_2 nanoparticles and films and their performance for photocurrent response under UV illumination. J Alloys Compd 541:421–427. doi: 10.1016/j.jallcom.2012.07.010

El-Sharkawy EA, Al-Shihry SS, Youssef AM (2007) Structural characterization and catalytic activities of titania supported iron(III) oxide catalysts: effect of Li? impregnation. Mater Lett 61:2947–2951. doi: 10.1016/j.matlet.2006.10.044

EPA/600/R-09/057F (2010) Nanomaterial case studies: nano-scale titanium dioxide in water treatment and in topical sunscreen national centre for environmental assessment. RTP Division Office of Research and Development, US Environmental Protection Agency

Fabrega C, Andreu T, Cabot A, Ramon Morante J (2010) Location and catalytic role of iron species in TiO_2:Fe photocatalysts: an EPR study. J Photochem Photobiol A Chem 211:170–175. doi: 10.1016/j.jphotochem.2010.03.003

Fenoglio I, Greco G, Livraghi S, Fubini B (2009) Non-UV-induced radical reactions at the surface of TiO_2 nanopar-ticles that may trigger toxic responses. Chem Eur J 15:4614–4621. doi: 10.1002/chem.200802542

Fenoglio I, Fubini B, Ghibaudi EM, Turci F (2011) Multiple aspects of the interaction of biomacromolecules with inorganic surfaces. Adv Drug Deliv Rev 63:1186–1209. doi: 10.1016/j.addr.2011.08.001

Fenoglio I, Ponti J, Alloa E, Ghiazza M, Corazzari I, Capo-maccio R, Rembges D, Oliaro-Bosso S, Rossi F (2013) Singlet oxygen plays a key role in the toxicity and DNA damage of nanometric TiO_2 to human keratinocytes. Nanoscale 5:6567–6576

Fujishima A, Zhang X, Tryk DA (2008) TiO(2) photocatalysis and related surface phenomena. Surf Sci Rep 63:515–582. doi: 10.1016/j.surfrep.2008.10.001

Gedik CM, Boyle SP, Wood SG, Vaughan NJ, Collins AR (2002) Oxidative stress in humans: validation of bio-markers of DNA damage. Carcinogenesis 23:1441–1446. doi: 10.1093/carcin/23.9.1441

George S, Pokhrel S, Ji Z, Henderson BL, Xia T, Li L, Zink JI, Nel AE, Maedler L (2011) Role of Fe doping in tuning the band gap of TiO_2 for the photo-oxidation-induced cyto-toxicity paradigm. J Am Chem Soc 133:11270–11278. doi: 10.1021/ja202836s

Gerloff K, Fenoglio I, Carella E, Kolling J, Albrecht C, Boots A, Fo¨rster I, Schins R (2012) Distinctive toxicity of TiO_2 rutile/anatase mixed phases nanoparticles on Caco-2 cells Chem. Res Toxicol 2012(25):646–655. doi: 10.1021/tx200334k

Ghiazza M, Scherbart AM, Fenoglio I, Grendene F, Turci F, Martra G, Albrecht C, Schins RPF, Fubini B (2011) Surface iron inhibits quartz-induced cytotoxic and inflammatory responses in alveolar macrophages. Chem Res Toxicol 24:99–110. doi: 10.1021/tx1003003

Ghiazza M, Carella E, Oliaro-Bosso S, Corazzari I, Viola V, Fenoglio I (2013) Predictive tests to evaluate oxidative potential of engineered nanomaterials. J Phys Conf Ser 429:012024. doi: 10.1088/1742-6596/429/1/012024

Jaeger A, Weiss DG, Jonas L, Kriehuber R (2012) Oxidative stress-induced cytotoxic and genotoxic effects of nano-sized titanium dioxide particles in human HaCaT keratinocytes. Toxicology 296:27–36. doi: 10.1016/j.tox.2012.02.016

Jin Q, Fujishima M, Tada H (2011) Visible-light-active iron oxide-modified anatase titanium(IV) dioxide. J Phys Chem C 115:6478–6483. doi: 10.1021/jp201131t

Kagan VE, Tyurina YY, Tyurin VA, Konduru NV, Potapovich AI, Osipov AN, Kisin ER, Schwegler-Berry D, Mercer R, Castranova V, Shvedova AA (2006) Direct and indirect effects of single walled carbon nanotubes on RAW 264.7 macrophages: role of iron. Toxicol Lett 165:88–100

Kim JI, Lee JH, Choi DS, Won BM, Jung MY, Park J (2009) Kinetic study of the quenching reaction of singlet oxygen by common synthetic antioxidants (tert-butylhydroxyanisol, tert-di-butylhydroxytoluene, and tert-butylhydroquinone) as compared with alpha-tocopherol. J Food Sci 74:C362. doi: 10.1111/j.1750-3841.2009.01160.x

Konaka R, Kasahara E, Dunlap WC, Yamamoto Y, Chien KC, Inoue M (1999) Irradiation of titanium dioxide generates both singlet oxygen and superoxide anion. Free Radic Biol Med 27:294–300. doi: 10.1016/s0891-5849(99)00050-7

Landsiedel R, Ma-Hock L, Van Ravenzwaay B, Schulz M, Wiench K, Champ S, Schulte S, Wohlleben W, Oesch F (2010) Gene toxicity studies on titanium dioxide and zinc oxide nanomaterials used for UV-protection in cosmetic formulations. Nanotoxicology 4:364–381. doi: 10.3109/17435390.2010.506694

Lee WA, Pernodet N, Li B, Lin CH, Hatchwell E, Rafailovich MH (2007) Multicomponent polymer coating to block photocatalytic activity of TiO(2) nanoparticles. Chem Commun 7:4815–4817. doi: 10.1039/b709449c

Lund LG, Aust AE (1990) Iron mobilization from asbestos by chelators and ascorbic-acid. Arch Biochem Biophys 278:60–64

Lutterotti L, Matthies S, Wenk HR, Schultz AS, Richardson JW (1997) Combined texture and structure analysis of deformed limestone from time-of-flight neutron diffraction spectra. J Appl Phys 81:594–600. doi: 10.1063/1.364220

Magdolenova Z, Bilanicova D, Pojana G, Fjellsbo LM, Hudecova A, Hasplova K, Marcomini A, Dusinska M (2012) Impact of agglomeration and different dispersions of titanium dioxide nanoparticles on the human related in vitro cytotoxicity and genotoxicity. J Environ Monit 14:455–464. doi: 10.1039/c2em10746e

Pal B, Sharon M, Nogami G (1999) Preparation and characterization of TiO(2)/Fe(2)O(3) binary mixed oxides and its photocatalytic properties. Mater Chem Phys 59:254–261. doi: 10.1016/s0254-0584(99)00071-1

Park H-O, Yu M, Kang SK, Yang SI, Kim Y-J (2011) Comparison of cellular effects of titanium dioxide nanoparticles with different photocatalytic potential in human keratino-cyte, HaCaT cells. Molec Cell Toxicol 7:67. doi: 10.1007/ s13273-011-0010-4

Pfannschmidt C, Langowski J (1998) Superhelix organization by DNA curvature as measured through site-specific labeling. J Mol Biol 275:601–611

Pulskamp K, Diabate S, Krug HF (2007) Carbon nanotubes show no sign of acute toxicity but induce intracellular reactive oxygen species in dependence on contaminants. Toxicol Lett 168:58–74. doi: 10.1016/j.toxlet.2006.11.001 Radecka M, Rekas M, Trenczek-Zajac A, Zakrzewska K (2008) Importance of the band gap energy and flat band potential for application of modified TiO_2 photoanodes in water photolysis. J Power Sources 181:46–55. doi: 10.1016/j.jpowsour.2007.10.082

Rehman S, Ullah R, Butt AM, Gohar ND (2009) Strategies of making TiO_2 and ZnO visible light active. J Hazard Mater 170:560–569. doi: 10.1016/j.jhazmat.2009.05.064

Ricci A, Chretien MN, Maretti L, Scaiano JC (2003) TiO_2-promoted mineralization of organic sunscreens in water suspension and sodium dodecyl sulfate micelles. Photochem Photobiol Sci 2:487–492. doi: 10.1039/b212815b

Sacco MG, Pariselli F, Rembges D (2010) A model to evaluate biological effects from combined exposure to UVa/b radiation and toluene. Fresenius Environ Bull 19:330–338 Sanders K, Degn LL, Mundy WR, Zucker RM, Dreher K, Zhao B, Roberts JE, Boyes WK (2012) In vitro phototoxicity and hazard identification of nano-scale titanium dioxide. Toxicol Appl Pharmacol 258:226–236. doi: 10.1016/j.taap.2011.10.023

Sayes CM, Wahi R, Kurian PA, Liu YP, West JL, Ausman KD, Warheit DB, Colvin VL (2006) Correlating nanoscale titania structure with toxicity: a cytotoxicity and inflam-matory response study with human dermal fibroblasts and human lung epithelial cells. Toxicol Sci 92:174–185. doi: 10.1093/toxsci/kfj197

Shoonen MAA, Cohn CA, Roemer E, Laffers R, Simon SR, O'Riordan T (2006) Mineral-induced formation of reactive oxygen species. In: Shai N, Schoonen MAA (eds) Medical Mineralogy and Geochemistry. Reviews in Mineralogy and Geochemistry, vol 64. The Mineralogical Society of America, Chantilly, pp 179–222

Shukla RK, Sharma V, Pandey AK, Singh S, Sultana S, Dhawan A (2011) ROS-mediated genotoxicity induced by titanium dioxide nanoparticles in human epidermal cells. Toxicol In Vitro 25:231–241. doi: 10.1016/j.tiv.2010.11.008

Tiano L, Armeni T, Venditti E, Barucca G, Mincarelli L, Damiani E (2010) Modified TiO(2) particles differentially affect human skin fibroblasts exposed to UVA light. Free Radic Biol Med 49:408–415. doi: 10.1016/j.freeradbiomed. 2010.04.032

Turci F, Tomatis M, Lesci IG, Roveri N, Fubini B (2011) The iron-related molecular toxicity mechanism of synthetic asbestos nanofibres: a model study for high-aspect-ratio nanoparticles. Chem Eur J 17:350–358. doi: 10.1002/chem. 201001893

Wakefield G, Green M, Lipscomb S, Flutter B (2004) Modified titania nanomaterials for sunscreen applications: reducing

free radical generation and DNA damage. Mater Sci Technol 20:985–988. doi: 10.1179/016708304225019803 Wen L, Liu B, Zhao X, Nakata K, Murakami T, Fujishima A (2012) Synthesis, characterization, and photocatalysis of Fe-doped TiO_2: a combined experimental and theoretical study. Int J Photoenergy. doi: 10.1155/2012/368750

Xue C, Wu J, Lan F, Liu W, Yang X, Zeng F, Xu H (2010) Nano titanium dioxide induces the generation of ROS and potential damage in HaCaT cells under UVA irradiation. J Nanosci Nanotechnol 10:8500–8507. doi: 10.1166/jnn 2010.2682

Yaghoubi H, Taghavinia N, Alamdari EK (2010) Self cleaning TiO_2 coating on polycarbonate: surface treatment, photocatalytic and nanomechanical properties. Surf Coat Technol 204:1562–1568. doi: 10.1016/j.surfcoat.2009.09.085

Yu J, Xiang Q, Zhou M (2009) Preparation, characterization and visible-light-driven photocatalytic activity of Fe-doped titania nanorods and first-principles study for electronic structures. Appl Catal B Environ 90:595–602. doi: 10.1016/ j.apcatb.2009.04.021

Yu H, Irie H, Shimodaira Y, Hosogi Y, Kuroda Y, Miyauchi M, Hashimoto K (2010) An efficient visible-light-sensitive Fe(III)-grafted TiO_2 photocatalyst. J Phys Chem C 114:16481–16487. doi: 10.1021/jp1071956